

# Consistent increase of East Asian Summer Monsoon rainfall and its variability under climate change over China in CMIP6

Anja Katzenberger<sup>1,2</sup> and Anders Levermann<sup>1,2,3</sup>

<sup>1</sup>Potsdam Institute for Climate Impact Research, Potsdam, Germany

<sup>2</sup>Potsdam University, Potsdam, Germany

<sup>3</sup>LDEO, Columbia University, New York, USA

**Correspondence:** Anja Katzenberger (anja.katzenberger@pik-potsdam.de)

1 **Abstract.** The East Asia Monsoon (EAM) dominates the climate over the densely populated East China and adjacent regions  
2 and is therefore influencing a fifth of the world's population. Thus, it is highly relevant to assess the changes of the central  
3 characteristics of the East Asian Summer Monsoon (EASM) under future warming in the latest generation of coupled climate  
4 models of the Coupled Model Intercomparison Project Phase 6 (CMIP6). Using 34 CMIP6 models we show that all models that  
5 capture the EASM in the reference period 1995-2014 project an increase in June-August rainfall independent of the underlying  
6 emission scenario. The multi-model mean increase is 16.5% under SSP5-8.5, 11.8% under SSP3-7.0, 12.7% under SSP2-4.5  
7 and 9.3% under SSP1-2.6 in the period 2081-2100 compared to 1995-2014. For China, the projected monsoon increase is  
8 slightly higher (12.6% under SSP1-2.6 and 18.1% under SSP5-8.5). The EASM rainfall will particularly intensify in South-  
9 East China, Taiwan as well as North Korea. The ~~rainfall increase in South-East china is due to a northward shift of the southwest~~  
10 ~~winds associated with a northward shift of the ITCZ that strengthens the water supply towards this region. The~~ multi-model  
11 mean indicates a linear relationship of the EASM rainfall depending on the global mean temperature relatively independent  
12 of the underlying scenario: Per degree of global warming, the rainfall is projected to increase by 0.17mm/day which refers to  
13 3.1% of rainfall in the reference period. It is thus predominately showing a "wet-region-get-wetter" pattern. The changes in  
14 the wind fields in the region are relatively small indicating the minor importance of dynamic factors, while pointing towards  
15 thermodynamic factors as responsible for the rainfall increase. The interannual variability is also robustly projected to increase  
16 between 17.6% under SSP1-2.6 and 23.8% under SSP5-8.5 in the multi-model mean between 2050-2100 and 1965-2015.  
17 Comparing the same periods, extremely wet seasons are projected to occur 7.0-times more often under SSP5-8.5.

18 **Keywords:** East Asian Monsoon, Monsoon, CMIP6, climate models, China

## 19 1 Introduction

20 The climate over East Asia is dominated by the monsoon seasons which are defined as reversing seasonal winds between the  
21 Pacific Ocean and the East Asian continent associated with different rainfall regimes. Rainfall during the East Asian Summer  
22 Monsoon (EASM) accounts for 40–50% of the annual precipitation in South China and 60–70% of the annual precipitation in  
23 North China (Lei et al., 2011) making it a central factor for the socioeconomic livelihoods in the region.

24 During mid ~~may~~May, rainfall surges over the South China Sea establishing a planetary-scale monsoon rainband extending  
25 from the South Asian marginal seas to subtropical western North Pacific. The monsoon then gradually progresses towards  
26 inland resulting in the synchronized onset of the Indian monsoon season as well as the the monsoon season in China and Japan  
27 in early June (Wang et al., 2002). During the summer months, low level southerly winds transport moisture to East China,  
28 Korea and Japan where it converges within the rain belt that is called the Meiyu in China, the Baiu in Japan, and the Changma  
29 in Korea. The wind direction follows the pressure gradient resulting from a zonal land-sea thermal contrast varying throughout  
30 the course of a year (Ha et al., 2012; Wang et al., 2002). The rainfall reaches its maximum in late June over the Meiyu/Baiu and  
31 in late July over northern China. Then, the rainy season retreats progressively poleward in East Asia during July and August,  
32 while southward in the Indian summer monsoon (Wang et al., 2002).

33 Since the East Asian Monsoon is located in the subtropics - unlike other monsoon systems, it is additionally influenced by  
34 mid-latitude disturbances and convective activity (Ha et al., 2012). Besides, the EAM interacts with various climatological pat-  
35 terns on various time scales, including El Niño-Southern Oscillation (ENSO), the Arctic Oscillation (AO), the Indian summer  
36 monsoon, spring Eurasian snow cover and the thermal forcing of the Tibetan Plateau (Ha et al., 2012).

37 The progressing and retreat of the Meiyu belt is associated with a large variability of precipitation over East Asia and  
38 accompanied by floods and droughts with potentially devastating impacts on socioeconomic livelihood (Yihui et al., 2020).  
39 In June and July 2020 large parts of East and South Asia were flooded as a result of excessive monsoon rainfall affecting  
40 approx. 35 mio. individuals (Volonté et al., 2021). Therefore, assessing the climate model projections of the East Asian summer  
41 monsoon under climate change is of critical importance for national and regional management strategies.

42 The central approach to assess changes in the East Asian monsoon throughout the 21st century are global climate models.  
43 The general circulation models (GCM) participating in the Coupled Model Intercomparison Project (CMIP) have provided  
44 some insight regarding future changes of the EAM. The models from the previous generation (CMIP5) project an increase of  
45 the East Asian Monsoon of 10–15% throughout the 21st century under RCP6.0, most pronounced over the Baiu region and  
46 over the north and northeast of the Korean Peninsula (Seo et al., 2013). The strengthening of monsoon rainfall is attributed to an  
47 increase in evaporation as well as moist flux convergence induced by the (north) westward shift of the North Pacific subtropical  
48 high (Lee and Wang, 2014; Seo et al., 2013). Besides, the CO<sub>2</sub>-induced strengthening of the land-sea thermal contrast plays a  
49 central role for the Asian monsoon (Endo et al., 2018). Chen and Sun (2013) find that the frequency and intensity of intense  
50 precipitation events are also projected to significantly increase over East Asia under RCP4.5.

51 The continuous development of the GCMs in CMIP has also lead to the improvement of the models' performance regarding  
52 the East Asian Monsoon. While most CMIP3 models show a limited capacity in simulating the precipitation over East Asian  
53 monsoon areas (Kai et al., 2009; Chen and Sun, 2013), the previous generation models of CMIP5 provided improvements  
54 regarding observed spatial and temporal precipitation patterns (Seo et al., 2013). Nevertheless, CMIP5 models struggle to  
55 reproduce rainfall bands around 30°N as well as the northward shift of the western North Pacific subtropical high (Huang  
56 et al., 2013).

57 Further progress has been made by CMIP6 models that outperform their predecessors regarding the EAM in past periods  
58 (Jiang et al., 2020; Xin et al., 2020; Yu et al., 2023). These improvements are related to the reduced biases in the sea surface

59 temperature (SST) over the Northwestern Pacific Ocean and better spatial resolution (Xin et al., 2020). In general, the CMIP6  
60 models have reliable abilities in capturing the main characteristics of the East Asian monsoon, including the spatial distribution  
61 of temperature and precipitation over China and the interannual variation (Xin et al., 2020; Masson-Delmotte et al., 2021).  
62 However GCMs simulate 16-80% more national rainfall compared to observations during 1979-2005 (Jiang et al., 2020).

63 Previous studies have compared CMIP5 and CMIP6 models for past periods (Jiang et al., 2020; Xin et al., 2020; Yu et al.,  
64 2023) or evaluated the changes of EASM in observations and CMIP6 models for 1979-2010 (Park et al., 2020) or analysed the  
65 inter-model spread for 1979-2014 (Huang et al., 2022). Other studies have analysed the CMIP6 projections for the EAM but  
66 only in the context of the global monsoon (Moon and Ha, 2020; Chen et al., 2020; Wang et al., 2020) and Asia monsoon (Ha  
67 et al., 2020) neglecting e.g. regional model performance. To the best of the authors' knowledge, no study has put the focus on  
68 the EAM providing detailed insight into projections for the EASM seasonal mean, its interannual variability as well as the oc-  
69 currence of extremely wet seasons for different time periods in the future under different emission scenarios. Besides, [expected](#)  
70 [changes in wind patterns due to global warming are poorly investigated in this region \(Bayhaqi et al., 2024\)](#). Additionally, we  
71 provide the central projections for China specifically, as highly relevant to policy makers. Here, we use the latest generation of  
72 climate models in order to update the projected changes of the EAM rainfall under different socioeconomic scenarios through-  
73 out the 21st century. For this purpose, we compare the available models and choose the ones with the best performance for the  
74 further analysis. Section 2 provides a brief overview of the underlying climate model data and the Methods. In Subsection 3.1,  
75 we identify the best performing models regarding the EASM among the available models. Subsection 3.2 presents the results  
76 of the mean summer monsoon precipitation, while Subsection 3.3 focuses on the long-term trend of interannual variability  
77 and Subsection 3.4 provides further insights regarding the frequency of extremely wet seasons. The results are discussed and  
78 concluded in Section 4.

## 79 **2 Methods**

80 In this study, we use 34 CMIP6 models that were available for the historic period (1850-2014) as well as for the future period  
81 (2015-2100) under SSP5-8.5 in ScenarioMIP (O'Neill et al., 2016; Tebaldi et al., 2020). Table 1 provides an overview of  
82 the models and their modelling centers. We use four scenarios (SSP1-2.6, SSP2-4.5, SSP3-7.0, SSP5-8.5) that are based on  
83 different socioeconomic pathways with their associated greenhouse gas emissions as well as aerosol pollution levels. These  
84 pathways are then translated into the resulting forcing levels (Van Vuuren et al., 2014; O'Neill et al., 2017). The resolution of  
85 the native grids in which the simulations were run are presented in Table A1 ranging from 2.5 to 500km. For the analysis, we  
86 regrid the model grids to uniform 1°longitude x 1°latitude grids by first order conservative remapping. We use one ensemble  
87 member per model (if available r1i1p1f1). Besides, we focus on the monsoon area over land in 20-50°N and 100-150°E.  
88 Monsoon area is defined as grid cells with summer (June-August) and winter (December-February) rainfall differing by a  
89 specific threshold as e.g. applied in the IPCC AR6 (Masson-Delmotte et al., 2021). We use 2 mm/day as a threshold to obtain a  
90 continuous area (See Fig. A1). For the analysis, we average the monthly rainfall data during the summer monsoon season from  
91 June to August.

**Table 1.** Overview of modeling center (group) and CMIP6 models. Only those models were selected for which data for the historical period and the SSP5-8.5 scenario was available at the time of the study.

Modeling Center (Group)	Model
Research Center for Environmental Changes, Academia Sinica (AS-RCEC)	Tai-ESM1
Alfred Wegener Institute (AWI)	AWI-CM-1-1-MR
Beijing Climate Center, China Meteorological Administration (BCC)	BCC-CSM2-MR
Chinese Academy of Meteorological Sciences (CAMS)	CAMS-CSM1-0
LASG, Institute of Atmospheric Physics, Chinese Academy of Sciences (CAS)	FGOALS-f3-L FGOALS-g3
Centre for Climate Change Research, Indian Institute of Tropical Meteorology (CCCR-IITM)	IITM-ESM
Canadian Centre for Climate Modelling and Analysis (CCCma)	CanESM5 CanESM5-CanOE
Euro-Mediterranean Centre for Climate Change (CMCC)	CMCC-ESM2 CMCC-CM2-SR5
Centre National de Recherches Météorologiques/ Centre Européen de Recherche et Formation Avancées en Calcul Scientifique (CNRM-CERFACS)	CNRM-ESM2-1 CNRM-CM6-1
Commonwealth Scientific and Industrial Research Organisation (CSIRO)	ACCESS-ESM1-5
Commonwealth Scientific and Industrial Research Organisation, ARC Centre of Excellence for Climate System Science (CSIRO-ARCCSS)	ACCESS-CM2
EC-Earth-Consortium	EC-Earth3 EC-Earth3-CC
Energy Exascale Earth System Model Project (E3SM-Project)	E3SM-1-1
First Institution of Oceanography (FIO-QLNM)	FIO-ESM-2-0
Institute of Numerical Mathematics (INM)	INM-CM4-8

Modeling Center (Group)	Model
Institut Pierre Simon Laplace (IPSL)	IPSL-CM6A-LR
Japan Agency for Marine-Earth Science and Technology/ Atmosphere and Ocean Research Institute, University of Tokyo (MIROC)	MIROC6 MIROC-ES2I
Met Office Hadley Centre (MOHC)	UKESM1-0-LL
Max Planck Institute for Meteorology (MPI-M)	MPI-ESM1-2-LR
Meteorological Research Institute (MRI)	MRI-ESM2-0 Y
National Center for Atmospheric Research (NCAR)	CESM2 CESM2-WACCM
Norwegian Climate Center (NCC)	NorESM2-MM
National Institute of Meteorological Sciences-Korea Met. Administration (NIMS-KMA)	KACE-1-0-G
NOAA Geophysical Fluid Dynamics Laboratory (NOAA-GFDL)	GFDL-CM4 GFDL-ESM4
Nanjing University of Information Science and Technology (NUIST)	NESM3

92 For the model evaluation, we use monthly precipitation data from the Global Precipitation Climatology Centre (GPCC) with  
93 a native grid of 1°longitude x 1°latitude grid for 1995-2014 as reference (Ziese et al., 2020). This data set is based on approx.  
94 85 0000 stations world-wide. For evaluating the models performance regarding the monsoon circulation, we use 850hPa wind  
95 data from the Japanese 55-year Reanalysis project (JRA-55) (Japan Meteorological Agency, 2013). In order to classify CMIP6  
96 models with better performance regarding the EASM, we apply the following selection criteria:

- 97 – The mean JJA rainfall is within two standard deviations of the observed mean in the GPCC dataset (1995-2014).
- 98 – The model’s standard deviation is within plus/minus 50 % of the observed GPCC standard deviation (1965-2014).
- 99 – The centered root mean square error (CRMSE) is smaller than 2 mm/day (1995-2014).
- 100 – The main features of the EASM circulation (southwest winds originated from the bay of Bengal and western flank of the  
101 tropical Western Pacific high) are captured according to the JRA-55 dynamics (1995-2014)

102 For the analysis of the projection, we use the future period from 2081-2100 and compare it to the reference period 1995-2014  
103 in accordance with the IPCC guidelines (Masson-Delmotte et al., 2021). For the analysis of the interannual variability and the  
104 occurrence of extremely wet seasons, we compare 2050-2100 to 1965-2014 in order to have longer time periods and robust  
105 results.

## 106 **3 Results**

### 107 **3.1 Model evaluation**

108 To evaluate the models' capacity in capturing the seasonal rainfall of the EASM in the past, we compare the mean seasonal  
109 rainfall to GPCP data in the period 1995-2014. The historical rainfall in the GPCP data is  $5.38 \pm 0.30$  mm/day. Only 14 out  
110 of 34 models are able to capture the historical mean within plus/minus two standard deviations while a majority of models  
111 have a tendency to overestimate the mean (Fig. 1). The mean of the models range from 3.94 mm/day (CAMS-CSM1-0) to  
112 7.89 mm/day (INM-CM4-8). The model EC-Earth3-CC captures the mean rainfall best. Besides, the CMIP6 models have the  
113 tendency to overestimate the interannual variability. The standard deviations of the model range from 0.22 mm/day (IPSL-  
114 CM6A-LR) to 0.64 mm/day (ACCESS-CM2). The results for all models are given in Table 2.

115 The rainfall during the EASM is strongest along coastal regions, particularly in South and East China, the Korean penin-  
116 sula, as well as Japan and Taiwan (See Fig. 2). The multi-model average of CRMSE is 1.97 mm/day with individual model  
117 results ranging from 1.24 (AWI-CM-1-1-MR) mm/day to 2.93 mm/day (TaiESM1). The results of the individual models are  
118 shown in Table 2. Seven models fulfill the MEAN, STD and CRMSE selection criteria, including two models of the EC-Earth  
119 Consortium. In order to avoid bias towards this model's center configuration, we only use EC-Earth3. For the remaining six  
120 models, the spatial rainfall distribution for 1995-2014 is given in Fig. 3. These models reproduce major spatial rainfall pat-  
121 terns including the rainfall in South China. Regarding the Korean peninsula, Taiwan and Japan, the models have a tendency to  
122 underestimate the local rainfall.

123 Fig. 4 shows the circulation during the EASM at 850hPa with strong south-west winds originating from the Bay of Bengal  
124 and the western flank of the tropical Western Pacific high. These main features are reproduced well from the models that fulfill  
125 the MEAN, STD and CRMSE criteria (Fig. 5). Therefore, we choose these six models as the CMIP6 models for the further  
126 analysis and refer to them as TOP6 models.

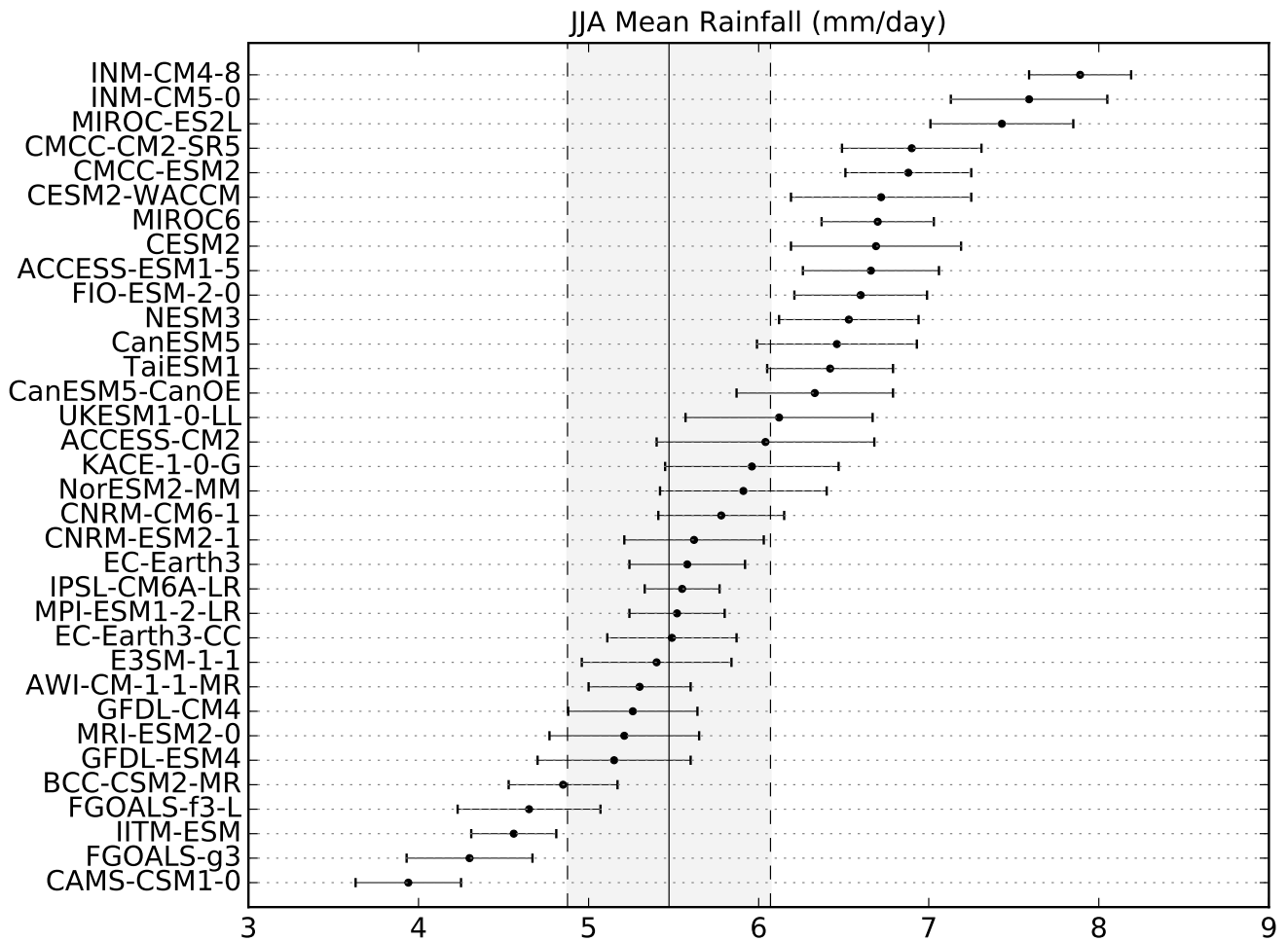


**Figure 1.** Mean Rainfall of the East Asian Summer Monsoon from June-September ( $\text{mm day}^{-1}$ ) over the region displayed in Fig. A1 from 34 CMIP6 models. The vertical line mark the mean monsoon rainfall from GPCP data (continuous line) plus/minus two standard deviations (dashed line). Circles with error bars represent mean plus/minus one standard deviation for each individual climate model during the same period.

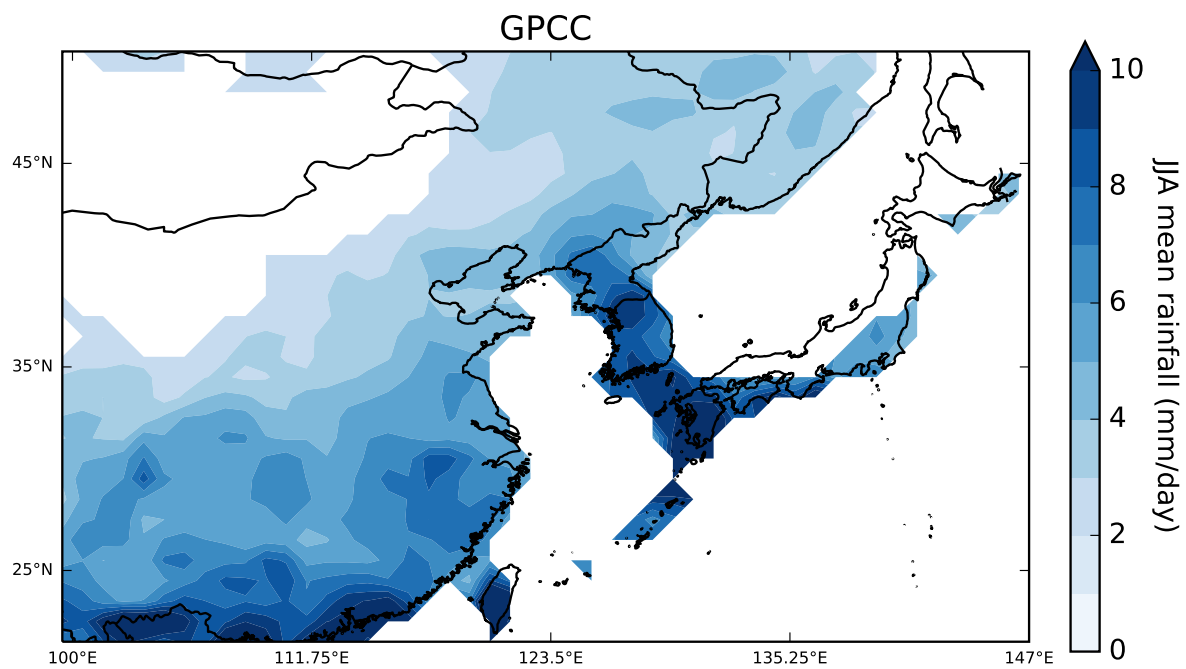


**Figure 2.** Spatial distribution of EASM averaged over the period 1995-2014 (GPCC data).



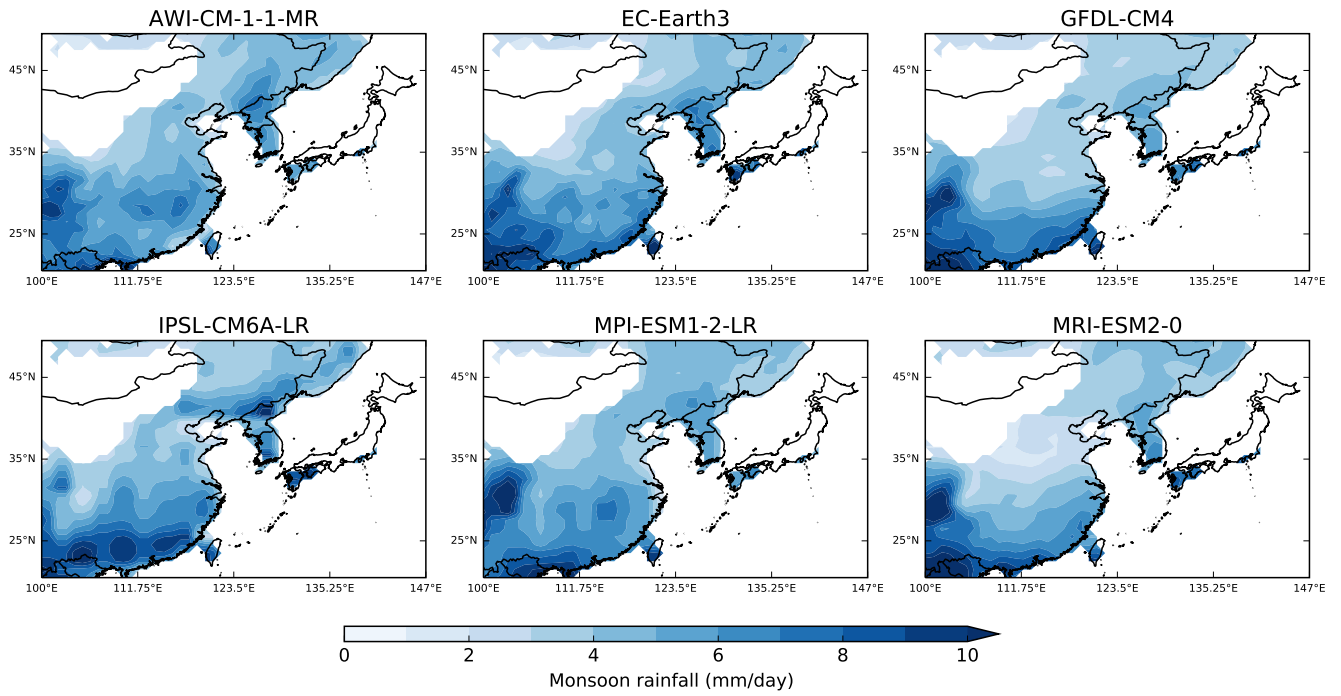


**Figure 3.** Spatial distribution of EASM averaged over the period 1995-2014 from the TOP6 CMIP6 models.

# JRA55 Reanalysis

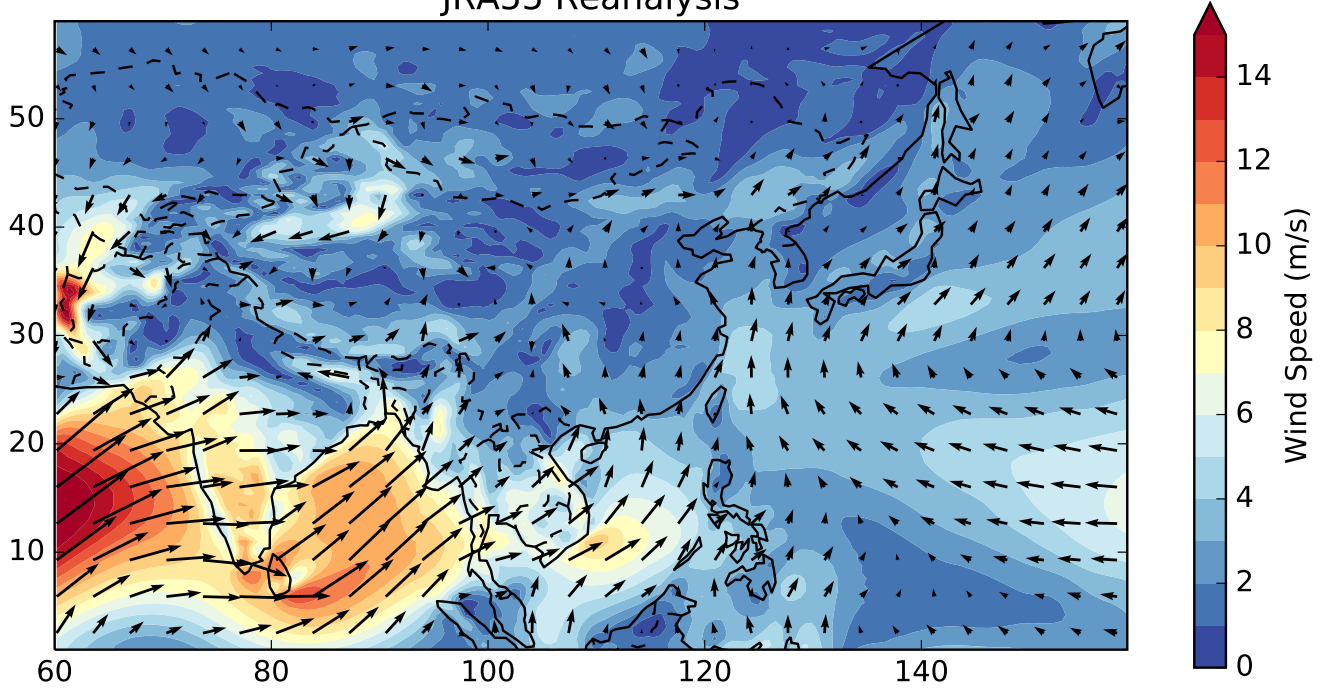


**Figure 4.** Wind vectors at 850hPa and wind speed (m/s) for 1995-2014 (JRA-55).

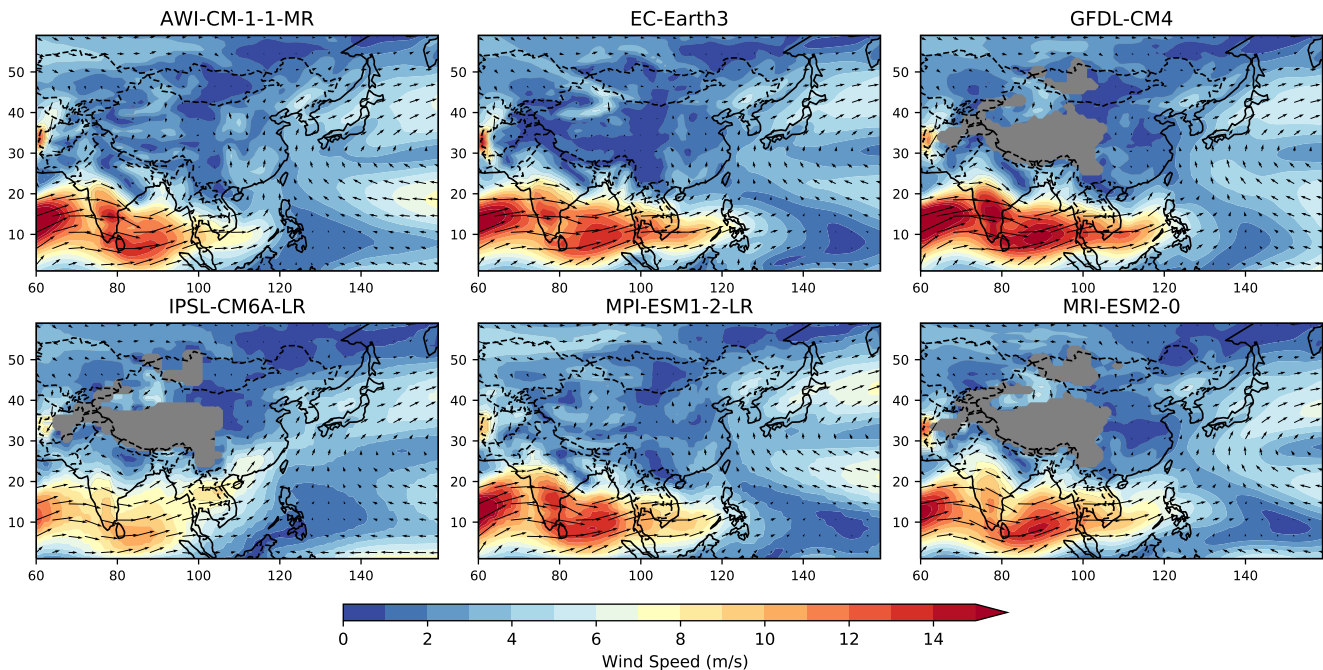


**Figure 5.** Wind vectors at 850hPa and wind speed (m/s) for 1995-2014 for the CMIP6 models with best performance regarding EASM (TOP6).

### 127 3.2 Seasonal mean rainfall

128 In order to analyse the long-term trend of the EASM under climate change, we provide the time series between 1850-2100  
 129 for all models under four emission scenarios for all models (Fig. 6) and TOP6 models only (Fig. A2). The multi-model mean  
 130 time series captures the decrease of rainfall in the second half of the 20th century resulting from increasing aerosol pollution.  
 131 This is followed by a rainfall increasing trend in the 21st century in all scenarios. The positive slopes in the scenarios vary,  
 132 potentially depending on the forcings resulting from the underlying socioeconomic pathway, particularly aerosols (reducing  
 133 effect on monsoon rainfall) and greenhouse gas emissions (enhancing effect on monsoon rainfall). High levels of development  
 134 and the focus on health and environmental concerns in SSP1, SSP2 and SSP5 result in reduced air pollution emissions in the  
 135 medium and long term, whereas SSP3 is characterized by weak aerosol control and slow development of air pollution policies.  
 136 This could explain why rainfall raises slower in SSP3 in the first half of the 21st century compared to other emission scenarios.

137 The timeseries for individual TOP6 models under SSP1-2.6 and SSP5-8.5 are shown in Fig. 7. All TOP6 models reproduce  
 138 the reducing effect of the EASM monsoon rainfall in the 20th century. However, in EC-Earth3 it is projected to occur in the  
 139 first half of the second century, while the other models capture the decline after the 1950s. All models projected an increase of  
 140 monsoon rainfall throughout the 21st century.

141 Under SSP5-8.5, SSP3-7.0, SSP2-4.5 and SSP1-2.6 all TOP6 models project an increase until 2081-2100 compared to 1995-  
 142 2014 (Fig. 8). The increase differs between the underlying emission scenarios: Under SSP5-8.5, the increase is 16.5% for the

143 multi-mean of TOP6 models (min: 6.2 %, max: 22.2%). Under SSP3-7.0, the TOP6 models project an average increase of  
144 11.8% (min: 10.3 %, max: 15.3%); Under SSP2-4.5, the increase projected is 12.7% (min: 6.6 %, max: 20.2%) and under  
145 SSP1-2.6, it is 9.3% (min: 6.7 %, max: 17.5%). These projected increasing tendencies are robust for all scenarios (The signal  
146 is classified as robust, where  $\geq 66\%$  of models show change greater than the variability threshold and  $\geq 80\%$  of all models  
147 agree on sign of change.) Further details regarding other periods (2021-2040, 2041-2060, 2061-2080) can be found in Table 3.  
148 Regarding the monsoon change only over China, the increase projected by TOP6 models is even stronger: Under SSP1-2.6 the  
149 monsoon rainfall intensifies by 12.6%, under SSP2-4.5 by 14.3%, under SSP3-7.0 by 17.8% and under SSP5-8.5 by 18.1% in  
150 multi-model average.

151 The spatial change in EASM rainfall between 2081-2100 and 1995-2014 based on the TOP6 multi-model mean is shown  
152 in Fig. 9. The majority of TOP6 models coincide in the larger scale rainfall change pattern. In most of the EASM region the  
153 rainfall is projected to increase in multi-model mean, particularly in Taiwan, South-East China as well as North Korea and  
154 adjacent regions. The increase in coastal regions is projected consistently by all TOP6 models (Fig. A3). However, particular  
155 increase in different regions differ in intensity. A decrease in rainfall is projected in parts of Guizhou and Chongqing. This  
156 decrease is present in all TOP6 models (Fig. A3), however with differing intensities. A weak decrease of rainfall over South  
157 Korea and South Japan is projected by three models.

158 Besides, we analyse the dependence of EASM rainfall on global mean temperature (GMT). The multi-model mean indicates  
159 a linear relationship relatively independent of the underlying emission scenario (Fig. 10). The projected average increase in  
160 daily rainfall during the monsoon season is 0.17mm per degree of global warming. This refers to an increase in EASM rainfall  
161 of 3.1% per degree GMT increase. The increase ranges from 0.08mm/day to 0.25mm/day depending on the TOP6 model.

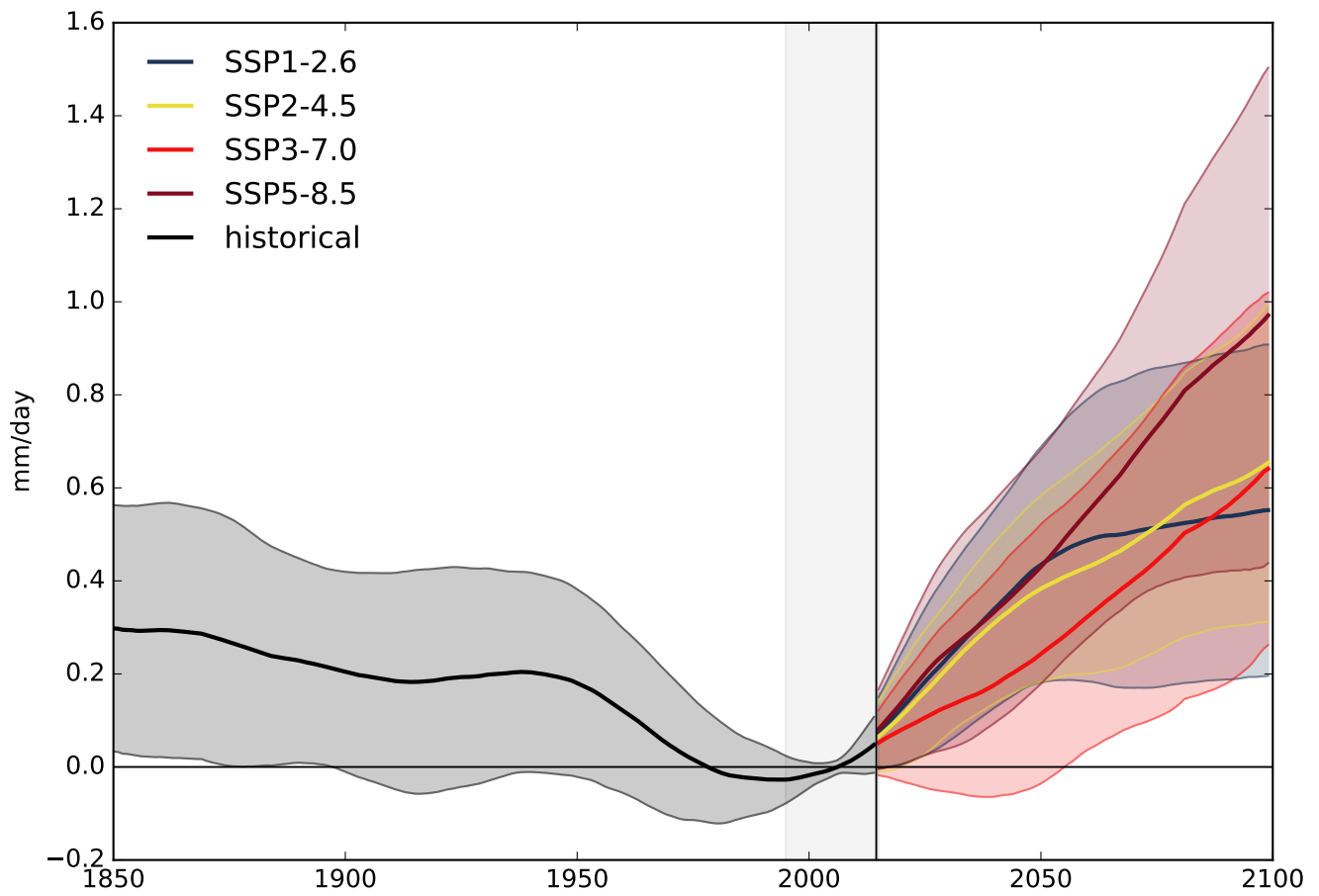


**Figure 6.** Timeseries of EASM ( $\text{mm } d^{-1}$ ) for the period 1850-2100 based on the multi-model mean of all 34 CMIP6 models relative to the period 1995-2014. The time series for individual models is smoothed using a singular spectrum analysis with a window size of 20 years before calculating the multi-model mean. For the method, see Golyandina and Zhigljavsky (2013). The shading marks the range of plus/minus one standard deviation.

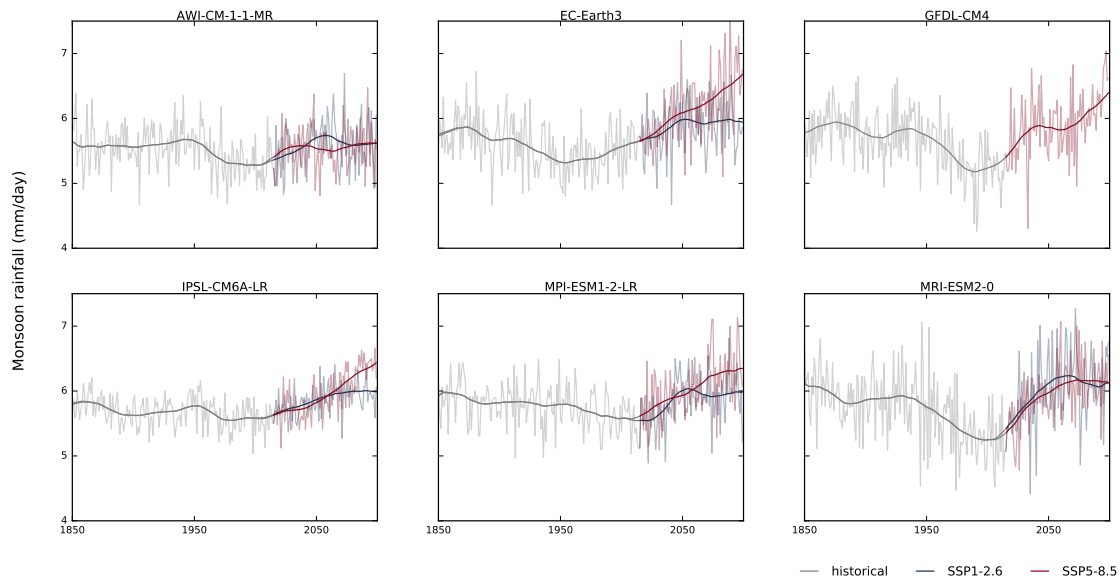


**Figure 7.** Timeseries of EASM (mm/day) for the period 1850-2100 from the TOP6 models. Transparent lines represent the annual values; bolt lines mark the trend obtained from a singular spectrum analysis with a window size of 20 years. For the method, see Golyandina and Zhigljavsky (2013).

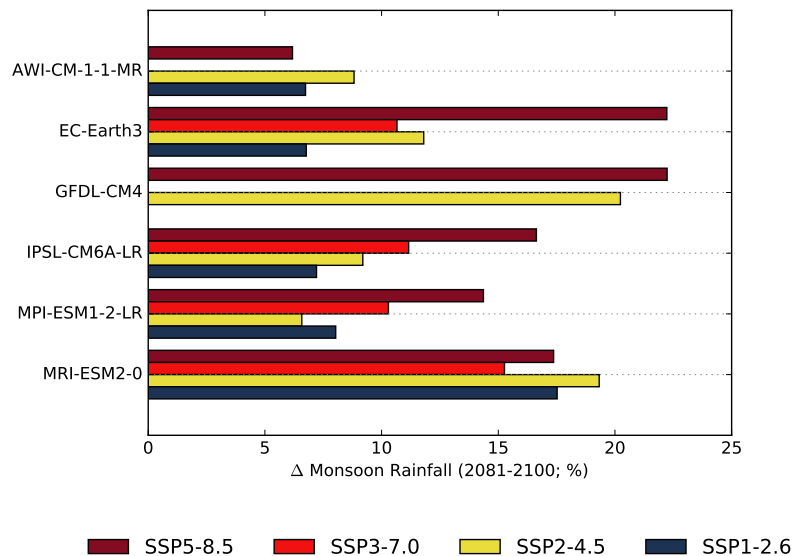


**Figure 8.** Projected increase (%) in monsoon rainfall until 2081-2100 compared to 1995-2014 (GPC) for the TOP6 models as available for the four emission scenarios.

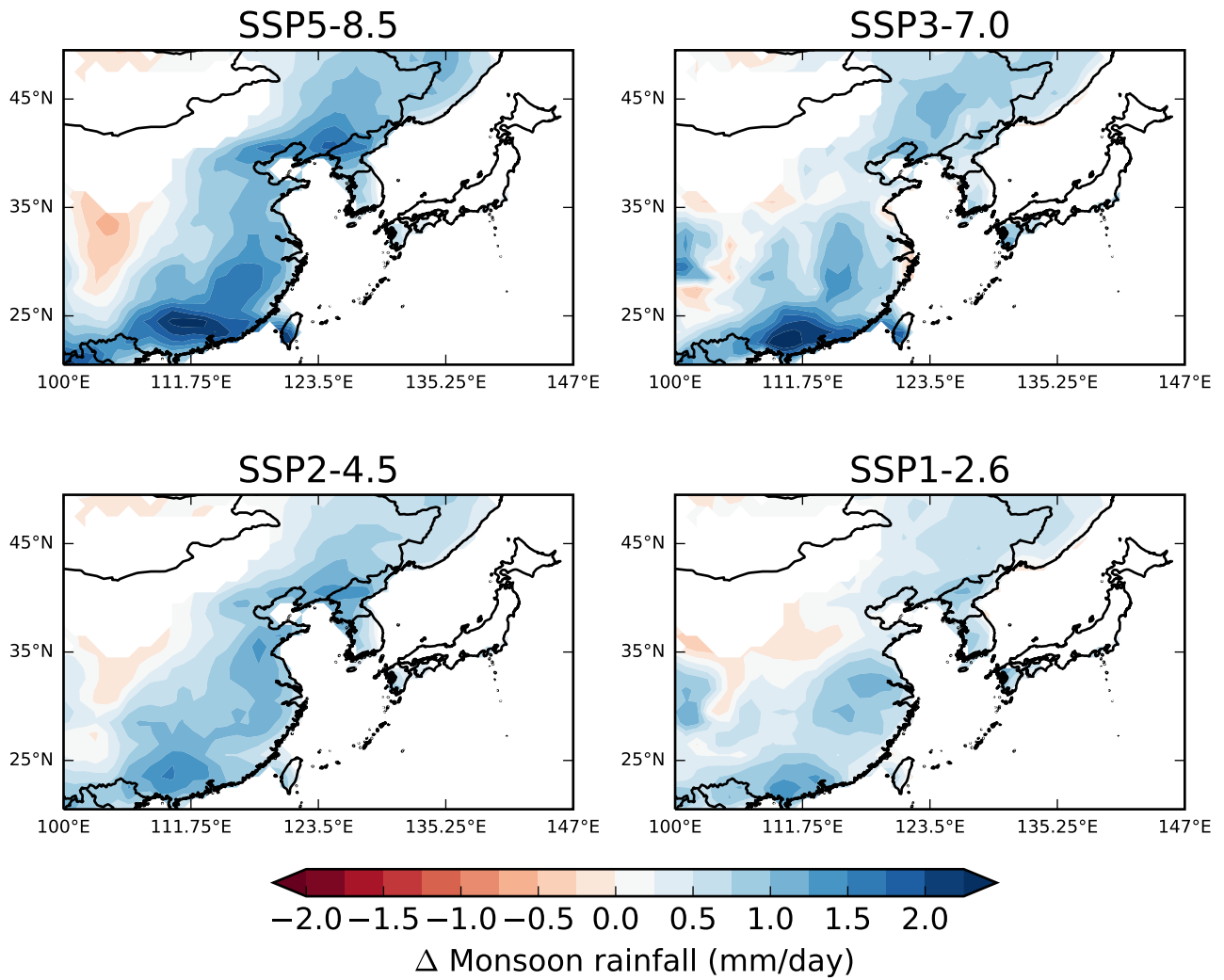


**Figure 9.** Spatial changes in JJA rainfall between 2081-2100 and 1995-2014 for multi-model mean of TOP6 models. The individual model results are shown in Fig. A3.

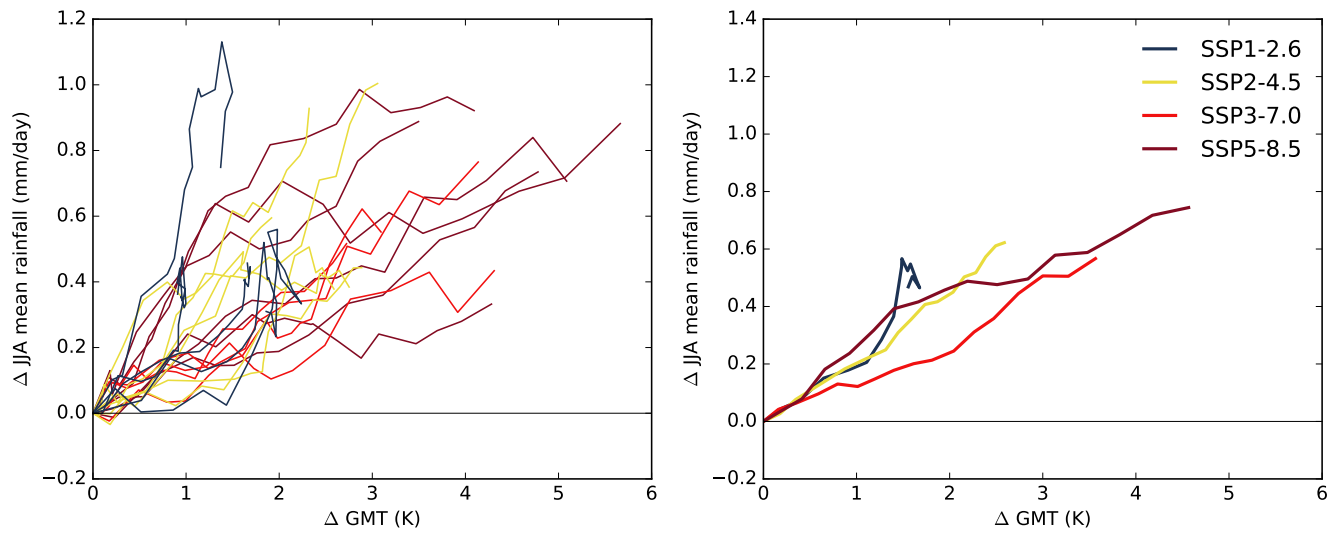


**Figure 10.** Change of EASM rainfall (mm/day) depending on change in global mean temperature (K) during the 21st century for all TOP6 models (left) and their multi-model average (right). The change is shown based on 20-year periods (1995-2015, 2000-2020, 2005-2025,...). Dashed gray lines indicate the slope. The reference period is 1995-2014.



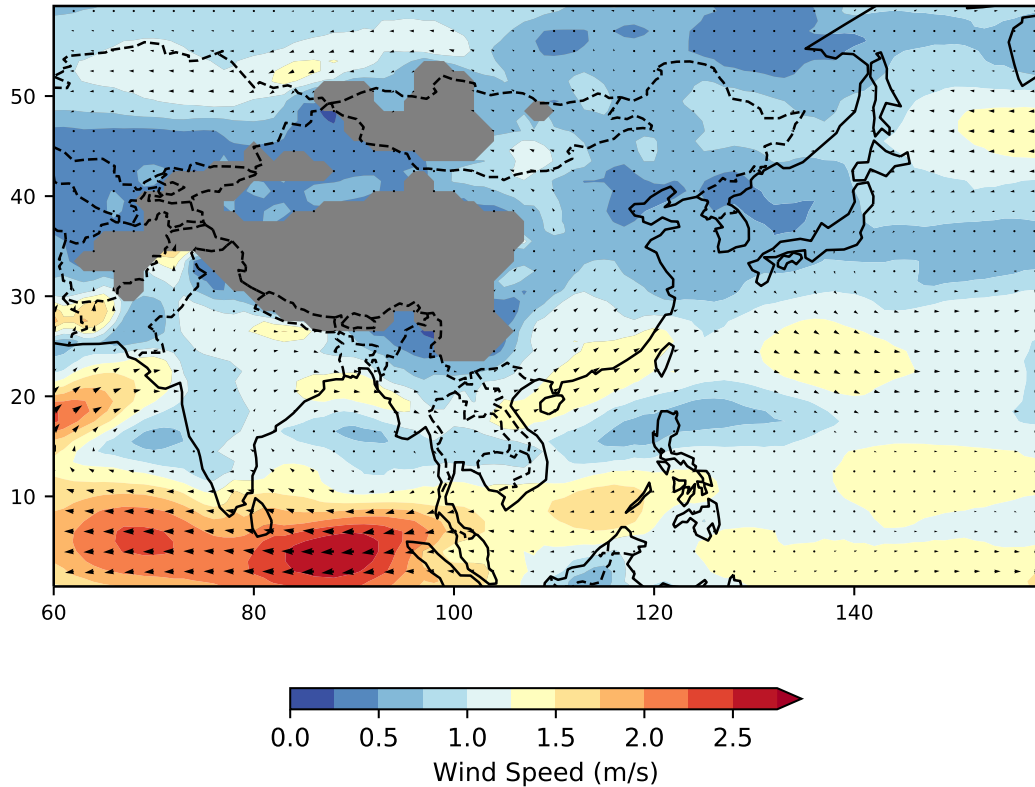


**Figure 11.** Change in wind vectors (850hPa) and wind speed (m/s) in 2081-2100 (SSP5-8.5) compared to the reference period. The multi-model mean of the TOP6 models is shown. Individual model results are presented in Fig. A4.

163 The TOP6 multi-model mean ~~projects that the~~ in the region of the EASM shows only minor changes in the local circulation  
 164 under SSP5-8.5 (Fig. 11). This indicates relatively weak dynamic changes and points towards dominating changes in thermodynamic  
 165 factors. The individual models confirm this pattern: AWI-CM-1-1-MR, IPSL-CM6A-LR, MRI-ESM2-0 and GFDL-CM4  
 166 mostly project changes of wind speed below 1.5 m/s. Only EC-Earth3 and MPI-ESM1-2-LR project slightly higher changes,  
 167 but are mostly not exceeding 2.5 mm/day. The most prominent feature in the wind change pattern are the northeastward winds  
 168 over the Bay of Bengal in 0-10°N will that weaken by up to 3m/s in the multi-model mean, while they will intensify in 0-  
 169 20°N(Fig. 11). This indicates a northward shift of these southwest winds and strengthens the moisture supply to South China  
 170 where an increase in rainfall is projected by 5 out of 6 models. This shift in wind patterns is associated with a northward shift  
 171 of the ITCZ originated in the warming land temperatures due to climate change. The most intense wind change is projected by  
 172 EC-Earth3 and. This change is present in all TOP6 models under SSP5-8.5 with most pronounced changes in IPSL-CM6A-LR  
 173 and the only model that does not project this trend is MRI-ESM2-0EC-Earth3.

174 Additionally, half of the TOP6 models (EC-Earth3, GFDL-CM4, MPI-ESM1-2-LR) project that the southwinds originated  
 175 in the South China Sea will have an increasing tendency towards east. However, this is not a robust finding given the strong  
 176 intermodel spread in this region.

### 177 3.4 Interannual variability

178 Furthermore, we analyse the interannual variability of the EASM rainfall. For this purpose, we remove the nonlinear trend  
 179 obtained by the singular spectrum analysis (see Fig. 7) and use the percentage changes in standard deviation between 2050-  
 180 2100 and 1965-2015. Under SSP5-8.5, all TOP6 models project an increase of interannual variability with a multi-mean of  
 181 23.8% (robust) ranging from 2.9% to 76.47% (Fig. 12). Under SSP3-7.0, 2/4 TOP6 models project an increase (not robust).  
 182 The multi-model mean is 9.0% (min: -22.8%, max: 48.1%). Under SSP2-4.5, 5/6 project increasing variability with an average  
 183 of 6.5% (min: -9.1%, max: 19.1%) and under SSP1-2.6, an increase is projected by 6/6 TOP6 models with a multi-model  
 184 average of 17.6% (min: 8.5%, max: 22.6%).

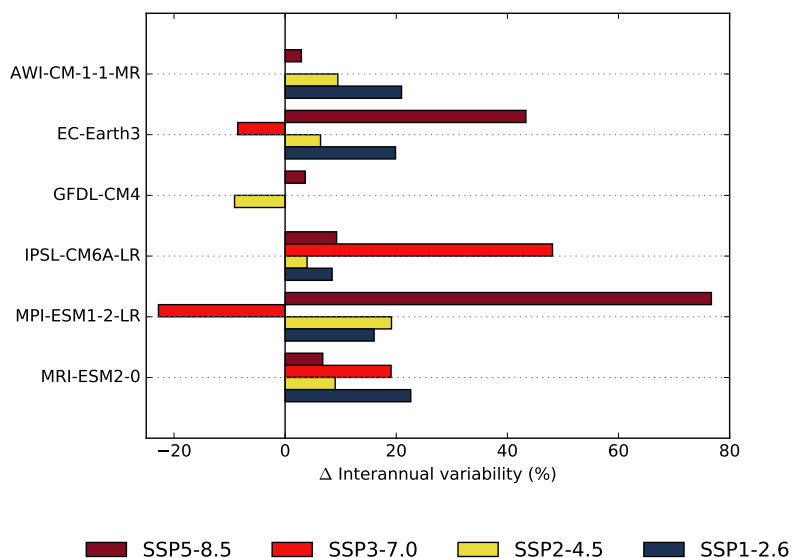


**Figure 12.** Change [%] of interannual variability between 2050-2100 and 1965-2015 for the EASM seasonal rainfall under four emission scenarios for the TOP6 models.

### 185 3.5 Extremely wet seasons

186 We use the 90th percentile for the period 1965-2015 in order to define extremely wet monsoon seasons. Thus, per definition  
 187 5 out of 50 years were extremely wet during the 50-years period from 1965-2015. Under SSP5-8.5, the number of extremely  
 188 wet monsoon seasons will increase by a factor of 7.0 until 2050-2100 according to the multi-model mean of TOP6 models.  
 189 Respectively, 35.2 years are expected to be extremely wet in 2050-2100 with individual TOP6 model projections ranging from

190 22 to 42 out of 50 seasons. Under SSP3-7.0, the multi-model mean projection is 29.0 ranging from 22 to 39 extremely wet  
 191 seasons. Under SSP2-4.5, 31.3 seasons in the future period are projected to be extremely wet ranging from 25 to 40. Under  
 192 SSP1-2.6 the multi-model mean projection is 28.6 ranging from 22 to 36 seasons. The increase over time is shown in Fig. 13.

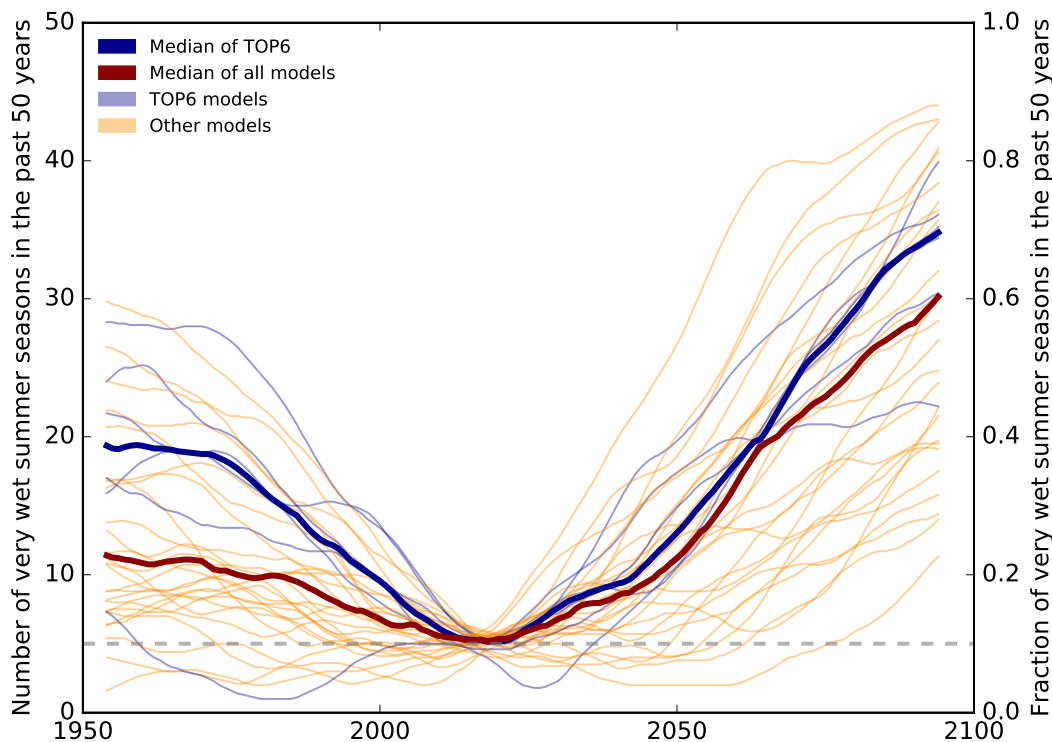


**Figure 13.** Increase of extremely wet monsoon seasons under unabated climate change (SSP5-8.5). TOP6 models are shown in blue, other CMIP6 models in orange. The reference period is 1965-2015 where per definition 5 out of 50 years were extremely wet.

#### 193 4 Discussion and Conclusion

194 In this study, we use 34 CMIP6 models in order to analyse their future projections under climate change regarding the East  
 195 Asian Summer Monsoon. We identify models that capture the EASM characteristics in the reference period best as TOP6  
 196 models and use them for our main analysis. The CMIP6 models have a tendency to overestimate the EASM rainfall which is in  
 197 line with previous studies (Jiang et al., 2020). This is different from other Asian monsoon regions, e.g. in the Indian monsoon  
 198 region models tend to underestimate the seasonal rainfall (Katzenberger et al., 2021, 2022). All TOP6 models robustly project  
 199 an increase of rainfall under all four emission scenarios. The projected multi-model mean increase until 2081-2100 is 16.5%  
 200 under SSP5-8.5, 11.8% under SSP3-7.0, 12.7% under SSP2-4.5 and 9.3% under SSP1-2.6. The rainfall-intensifying tendency is  
 201 also [confirmed](#) [confirming the results presented](#) by the IPCC, AR6 classifying the increasing trend as 'highly certain' (Masson-  
 202 Delmotte et al., 2021). The projected increase is also in line with CMIP5 projections, though even stronger increases are

203 projected in CMIP6 (Qu et al., 2014; Chen and Sun, 2013; Kitoh et al., 2013). But it has to be noted, that there are differences  
204 in the methods between the studies, preventing direct comparison of the results. The projections for the near-term depend on  
205 the implementation and efficiency of future air pollution control that is difficult to predict (Wilcox et al., 2020) adding further  
206 uncertainty. The increase in rainfall will particularly contribute to rainfall in South East China, Taiwan as well as North Korea -  
207 regions that are already experiencing a relatively strong monsoon. Thus the wet-regions-get-wetter dynamics is predominantly  
208 confirmed for the EASM in line with CMIP5 results (Seo et al., 2013). Over China, the monsoon is projected to increase by  
209 12.6% under SSP1-2.6, under SSP2-4.5 by 14.3%, under SSP3-7.0 by 14.1% and under SSP5-8.5 by 19.1%. Per degree of  
210 global warming, the monsoon is projected to increase by 0.17mm/day which refers to 3.1% of the rainfall in the reference  
211 period. ~~The intensification of the EASM is resulting from the combined effects of an enhanced evaporation due to increased~~  
212 ~~sea surface temperatures, increased water vapour~~ multi-model mean in the wind pattern reveals relatively minor changes in the  
213 circulation in the region. This indicates that there are only small changes in the dynamic component within East Asia pointing to  
214 the dominant contribution from the thermodynamic component. Indeed, this is in line with the CMIP6 study of Li et al. (2021)  
215 who quantified the role of the different components contributing to the EASM increase throughout the 21st century. In East  
216 China (Japan and Korea Region) long-term, they quantify the change in moisture advection to be +9.6% (+9.2%), evaporation  
217 +19.9 % (+16.1%) and moisture convergence +70.6% (+74.4%). Additionally, they split the moisture convergence term into  
218 a term that relates to circulation changes (dynamic changes), one that refers to moisture content changes (thermodynamic  
219 changes) and a residual term that can be assumed to be small. In East China (Japan and Korea Region) long-term, the  
220 thermodynamic term clearly dominates with +98.1% (+153.0%) over the dynamic term of +3.0% (-34.9%). The authors  
221 find that the dynamic term might even be cancelled out due to the large intermodel spread (Li et al., 2021). This intermodel  
222 spread might also at least partly explain that the dynamic component has been found to contribute positively as well as moist  
223 ~~flux convergence~~ negatively to the budget (Wang et al., 2014; Li et al., 2015; Lee et al., 2017; Li et al., 2021). However, most  
224 studies coincide with the dominant thermodynamic role in the region (Li et al., 2015; Lee et al., 2017; Li et al., 2021). But  
225 there is also one study that finds that the dynamic component might be dominating in the region with 67% over the 33%  
226 of the thermodynamic component (Xue et al., 2023). However, as pointed out by the authors of this study, the projections  
227 are based on a single model (CESM2) that in our study was also not among the best performing regarding the EASM  
228 characteristics. The relevance of evaporation and moisture convergence has already been reported in the context of CMIP5  
229 (Seo et al., 2013; Qu et al., 2014). Seo et al. (2013) found that these changes are induced by the (north) westward shift of the  
230 North Pacific subtropical high(Seo et al., 2013; Qu et al., 2014). Additionally, the strengthening of the Along the northern  
231 and northwestern flank of the strengthened high, intensified southerly or southwesterly winds lead to an increase in moisture  
232 convergence, intensifying precipitation particularly over the Baiu region to the east of Japan and the continental region to the  
233 north of the Korean Peninsula. Qu et al. (2014) also add the increased vertical transport of moisture in the EASM region and the  
234 capacity of warmer air to hold more moisture following Clausius-Clapeyron as relevant contributing factors. In other studies,  
235 the role of the strengthening of the ~~land-sea thermal contrast under global warming contributes to the rainfall increase of Asian~~  
236 ~~monsoon systems (Endo et al., 2018). Xue et al. (2023) provide insides regarding the underlying contribution of changes in the~~  
237 ~~thermodynamic and dynamic components.~~ thermal contrast under global warming is discussed (Endo et al., 2018).

238 Besides, we analysed the interannual variability that is particularly important for societal and economic adaptation strate-  
239 gies, defining the necessary interannual flexibility for agricultural irrigation, ~~flooding~~ flood management, etc. The interannual  
240 variability is projected to increase by 17.6% under SSP1-2.6, 6.5% under SSP2-4.5, 9.0% under SSP3-7.0 and 23.8% under  
241 SSP5-8.5 from 1965-2015 to 2050-2100. Comparing the CMIP6 multi-mean results under SSP5-8.5 of 31.4% to CMIP3 results  
242 under the respective A2 scenario, the projected increase in CMIP3 of 19% is considerably weaker (Lu and Fu, 2010). Addition-  
243 ally, extremely wet monsoon seasons are projected to occur 7.0 times more often under SSP5-8.5 compared to the reference  
244 period. The increase of interannual variability of the seasonal rainfall is accompanied by increasing interannual variability of  
245 the western North Pacific subtropical high and East Asian upper-tropospheric jet (Lu and Fu, 2010). The projected changes  
246 in the characteristics of the EASM are of high socioeconomic relevance and should be taken into account in the management  
247 decisions for the 21st century.

**Table 2.** Overview of model evaluation results: JJA mean (mean), standard deviation (STD) and centered root mean squared error (CRMSE). TOP6 models are marked. GPCC data is given as a reference.

Model	MEAN	STD	CRMSE
GPCC data	5.14	0.28	0
INM-CM4-8	7.89	0.3	2.45
INM-CM5-0	7.59	0.46	2.51
MIROC-ES2L	7.43	0.42	2
CMCC-CM2-SR5	6.9	0.41	2.41
CMCC-ESM2	6.88	0.37	2.35
CESM2-WACCM	6.72	0.53	2.13
MIROC6	6.7	0.33	1.91
CESM2	6.69	0.5	2.08
ACCESS-ESM1-5	6.66	0.4	2.3
FIO-ESM-2-0	6.6	0.39	2.57
NESM3	6.53	0.41	2.09
CanESM5	6.46	0.47	3.06
TaiESM1	6.42	0.37	2.22
CanESM5-CanOE	6.33	0.46	3.04
UKESM1-0-LL	6.12	0.55	1.73
ACCESS-CM2	6.04	0.64	2.37
KACE-1-0-G	5.96	0.51	2.03
NorESM2-MM	5.91	0.49	1.65
CNRM-CM6-1	5.78	0.37	2.22
CNRM-ESM2-1	5.62	0.41	2.28
<b>EC-Earth3</b>	<b>5.58</b>	<b>0.34</b>	<b>1.43</b>
<b>IPSL-CM6A-LR</b>	<b>5.55</b>	<b>0.22</b>	<b>1.9</b>
<b>MPI-ESM1-2-LR</b>	<b>5.52</b>	<b>0.28</b>	<b>1.95</b>
EC-Earth3-CC	5.49	0.38	1.41
E3SM-1-1	5.4	0.44	2.05
<b>AWI-CM-1-1-MR</b>	<b>5.3</b>	<b>0.3</b>	<b>1.81</b>
<b>GFDL-CM4</b>	<b>5.2</b>	<b>0.38</b>	<b>1.77</b>
<b>MRI-ESM2-0</b>	<b>5.21</b>	<b>0.44</b>	<b>1.92</b>
GFDL-ESM4	5.15	0.45	1.73
BCC-CSM2-MR	4.85	0.32	1.73
FGOALS-f3-L	4.65	0.42	1.71
IITM-ESM	4.56	0.25	2.15
FGOALS-g3	4.3	0.37	2.73
CAMS-CSM1-0	3.94	0.31	2.08

**Table 3.** Projected changes (%) for JJA mean rainfall of TOP6 models under four emission scenarios for 2021-2040, 2041-2060, 2061-2080, 2081-2100 compared to 1995-2014 (GPCC data).

	2021-2040			2041-2060			2061-2080			2081-2100		
	Min	Mean	Max	Min	Mean	Max	Min	Mean	Max	Min	Mean	Max
SSP1-2.6	0.9	4.0	10.5	6.0	10.0	16.6	5.8	9.1	19.4	6.7	9.3	17.5
SSP2-4.5	1.2	4.2	8.6	5.4	8.1	11.8	7.0	10.1	14.9	6.6	12.7	20.2
SSP3-7.0	1.0	1.8	2.7	0.9	4.2	6.4	6.8	9.1	12.5	10.3	11.8	15.3
SSP5-8.5	2.3	7.2	12.7	5.1	8.9	14.6	4.0	11.6	18.2	6.2	16.5	22.2

248 [Appendix](#)

249 ~~East Asian summer monsoon area within 20–50°N and 100–150°E as covered in this study.~~



**Table A1.** Overview of the model resolutions of the native model grids in which the 34 CMIP models were run. For the analysis in this study, the models have been remapped to a 1°horizontal grid.

Model	Atmosphere [km]	Land [km]	Ocean [km]
Tai-ESM1	100	100	100
AWI-CM-1-1-MR	100	100	25
BCC-CSM2-MR	100	100	50
CAMS-CSM1-0	100	100	100
FGOALS-f3-L	100	100	100
FGOALS-g3	250	250	100
IITM-ESM	250	250	100
CanESM5	500	500	100
CanESM5-CanOE	500	500	100
CMCC-ESM2	100	100	100
CMCC-CM2-SR5	100	100	100
CNRM-ESM2-1	250	250	100
CNRM-CM6-1	250	250	100
ACCESS-ESM1-5	250	250	100
ACCESS-CM2	250	250	100
EC-Earth3	100	100	100
EC-Earth3-CC	100	100	100
E3SM-1-1	100	100	50
FIO-ESM-2-0	100	100	100
INM-CM4-8	100	100	100
INM-CM5-0	100	100	50
IPSL-CM6A-LR	250	250	100
MIROC6	250	250	100
MIROC-ES21	500	500	100
UKESM1-0-LL	250	250	100
MPI-ESM1-2-LR	250	250	250
MRI-ESM2-0	100	100	100
GISS-E2-1-G	250	250	100
CESM2	100	100	100
CESM2-WACCM	100	100	100

**Table A1.** Continued.

Model	Atmosphere [km]	Land [km]	Ocean [km]
NorESM2-MM	100	100	100
KACE-1-0-G	250	250	100
GFDL-CM4	100	100	25
GFDL-ESM4	100	100	50
NESM3	250	2.5	100

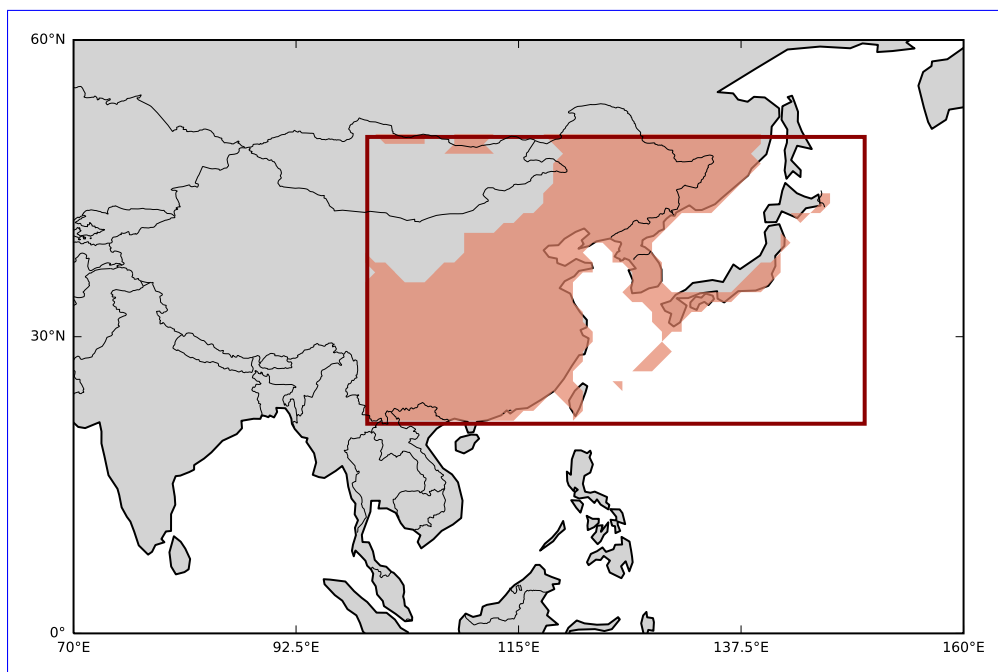


**Figure A1.** East Asian summer monsoon area within 20-50°N and 100-150°E as covered in this study.

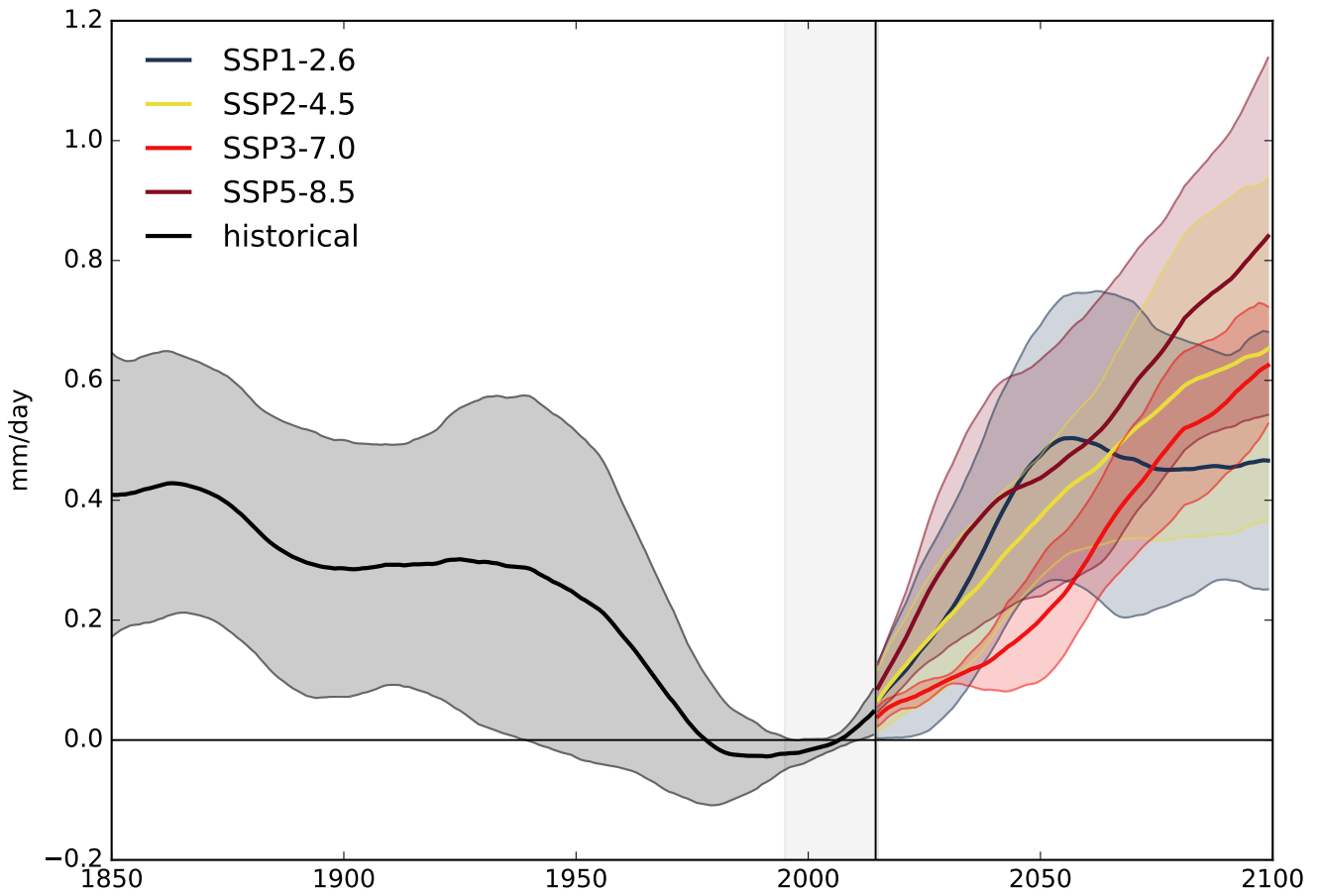


**Figure A2.** Timeseries of EASM ( $\text{mm d}^{-1}$ ) for the period 1850-2100 based on the multi-model mean of the TOP6 models relative to the period 1995-2014. The time series for individual models is smoothed using a singular spectrum analysis with a window size of 20 years before calculating the multi-model mean. For the method, see Golyandina and Zhigljavsky (2013). The shading marks the range of plus/minus one standard deviation.

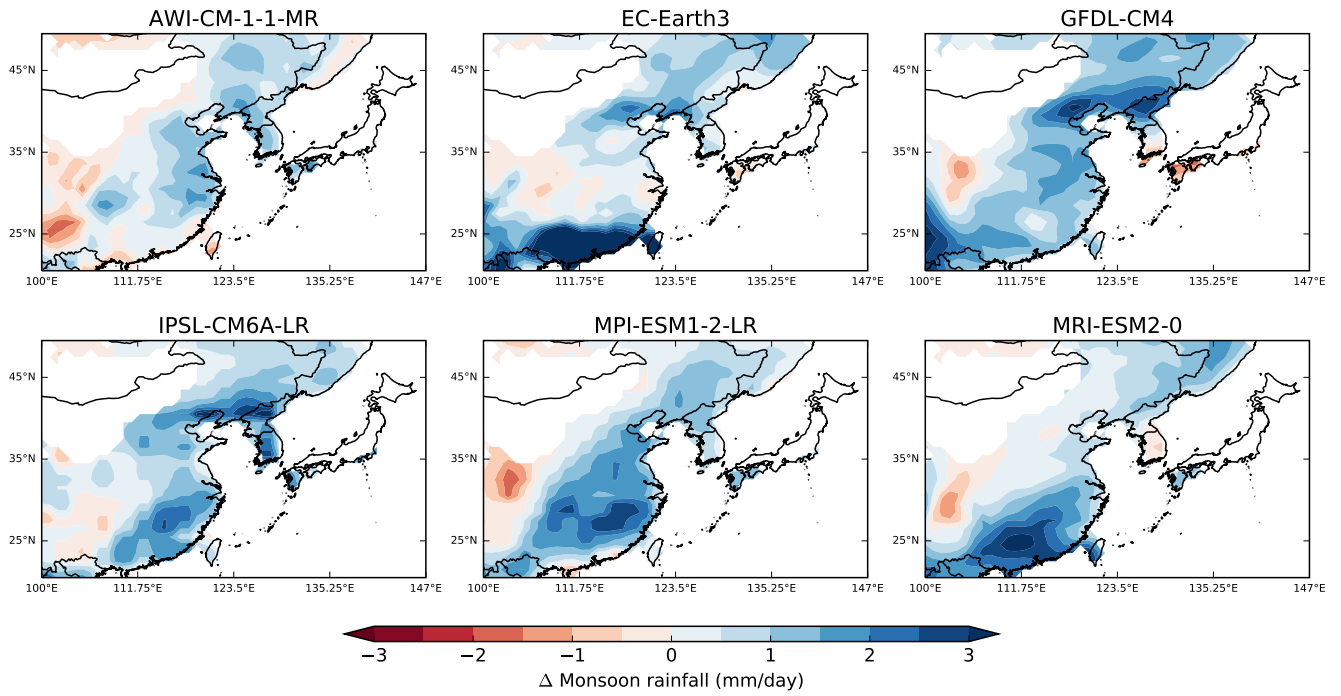


**Figure A3.** Spatial changes in JJA rainfall between 2081-2100 and 1995-2014 under SSP5-8.5 for TOP6 models. The multi-model mean is shown in Fig. 9.

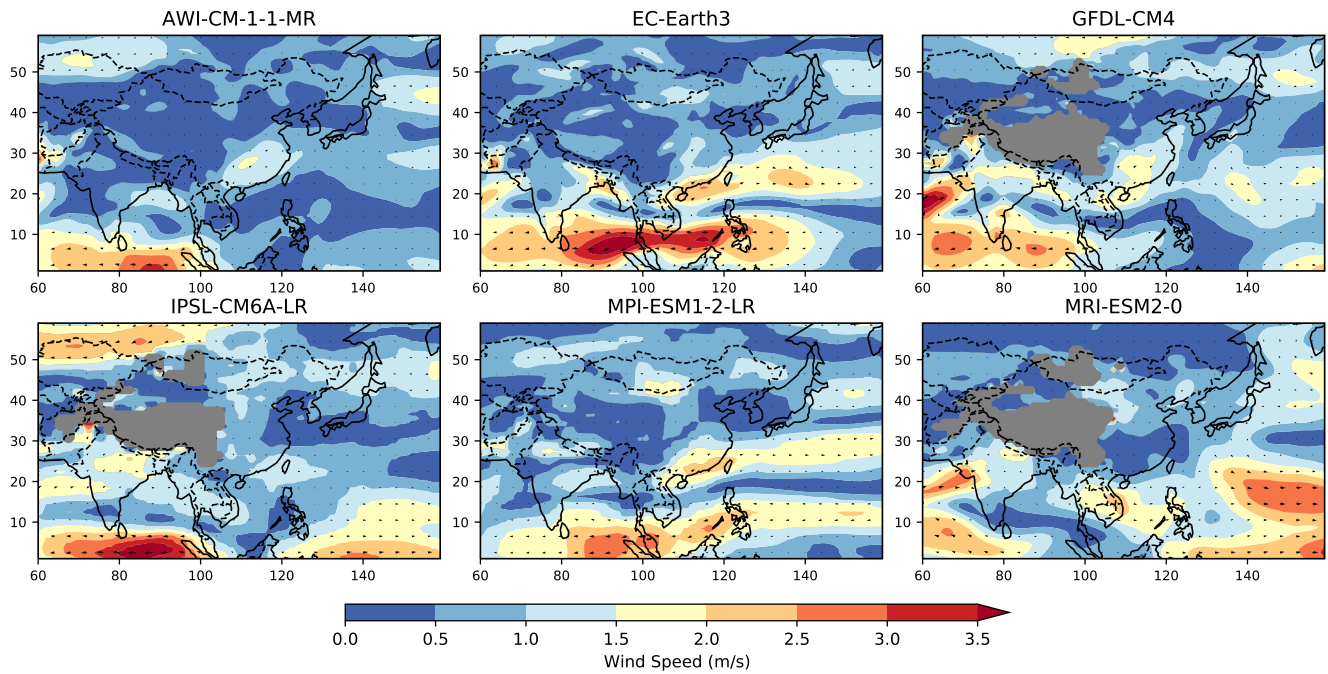


**Figure A4.** Change in wind vectors (850hPa) and wind speed (m/s) in 2081-2100 (SSP5-8.5) compared to the reference period.

## 250 **Statements and Declarations**

251 *Code and data availability.* The data sets from CMIP6 simulations are available via the CMIP6 Search Interface: [https://esgf-node.llnl.gov/](https://esgf-node.llnl.gov/search/cmip6/)  
252 [search/cmip6/](https://esgf-node.llnl.gov/search/cmip6/) (last access: 31 March 2023) (WCRP). The relevant CMIP6 data extract as well as the underlying code is available in a private  
253 github repository that will be made public and linked to zenodo when this article will be published.

254 *Funding:* The research was financially supported by the Heinrich-Boell Foundation who did not have any influence on the  
255 study design, the data analysis or the interpretation of the results (nor any other influence).

256 *Author contributions.* AL proposed the idea of this study. AK performed the analysis and wrote the paper. AK and AL discussed the results.

257 *Competing interests.* At least one of the (co-)authors is a member of the editorial board of Earth System Dynamics. The peer-review process  
258 was guided by an independent editor, and the authors have also no other competing interests to declare.

259 *Acknowledgements.* We acknowledge the World Climate Research Programme's Working Group on Coupled Modelling, which is respon-  
260 sible for CMIP, and we thank the climate modelling groups for producing and making available their model output. Besides, we thank the  
261 Copernicus Climate Change Service for providing the WFDE5 reanalysis data set.

## 262 **References**

- 263 Bayhaqi, A., Yoo, J., Jang, C. J., Kwon, M., and Kang, H.-W.: Near-Future Projection of Sea Surface Winds in Northwest Pacific Ocean  
264 Based on a CMIP6 Multi-Model Ensemble, *Atmosphere*, 15, 386, 2024.
- 265 Chen, H. and Sun, J.: Projected change in East Asian summer monsoon precipitation under RCP scenario, *Meteorology and Atmospheric*  
266 *Physics*, 121, 55–77, 2013.
- 267 Chen, Z., Zhou, T., Zhang, L., Chen, X., Zhang, W., and Jiang, J.: Global land monsoon precipitation changes in CMIP6 projections,  
268 *Geophysical Research Letters*, 47, e2019GL086 902, 2020.
- 269 Endo, H., Kitoh, A., and Ueda, H.: A unique feature of the Asian summer monsoon response to global warming: The role of different  
270 land–sea thermal contrast change between the lower and upper troposphere, *Sola*, 14, 57–63, 2018.
- 271 Golyandina, N. and Zhigljavsky, A.: *Singular Spectrum Analysis for time series*, Springer Science & Business Media, 2013.
- 272 Ha, K.-J., Heo, K.-Y., Lee, S.-S., Yun, K.-S., and Jhun, J.-G.: Variability in the East Asian monsoon: A review, *Meteorological Applications*,  
273 19, 200–215, 2012.
- 274 Ha, K.-J., Moon, S., Timmermann, A., and Kim, D.: Future changes of summer monsoon characteristics and evaporative demand over Asia  
275 in CMIP6 simulations, *Geophysical Research Letters*, 47, e2020GL087 492, 2020.
- 276 Huang, D., Liu, A., Zheng, Y., and Zhu, J.: Inter-Model Spread of the Simulated East Asian Summer Monsoon Rainfall and the Associated  
277 Atmospheric Circulations From the CMIP6 Models, *Journal of Geophysical Research: Atmospheres*, 127, e2022JD037 371, 2022.
- 278 Huang, D.-Q., Zhu, J., Zhang, Y.-C., and Huang, A.-N.: Uncertainties on the simulated summer precipitation over Eastern China from the  
279 CMIP5 models, *Journal of Geophysical Research: Atmospheres*, 118, 9035–9047, 2013.
- 280 Japan Meteorological Agency: JRA-55: Japanese 55-year Reanalysis, Monthly Means and Variances, <https://doi.org/10.5065/D60G3H5B>,  
281 2013.
- 282 Jiang, D., Hu, D., Tian, Z., and Lang, X.: Differences between CMIP6 and CMIP5 models in simulating climate over China and the East  
283 Asian monsoon, *Advances in Atmospheric Sciences*, 37, 1102–1118, 2020.
- 284 Kai, T., Zhong-Wei, Y., Xue-Bin, Z., and Wen-Jie, D.: Simulation of precipitation in monsoon regions of China by CMIP3 models, *Atmo-*  
285 *spheric and Oceanic Science Letters*, 2, 194–200, 2009.
- 286 Katzenberger, A., Schewe, J., Pongratz, J., and Levermann, A.: Robust increase of Indian monsoon rainfall and its variability under future  
287 warming in CMIP6 models, *Earth System Dynamics*, 12, 367–386, 2021.
- 288 Katzenberger, A., Levermann, A., Schewe, J., and Pongratz, J.: Intensification of very wet monsoon seasons in India under global warming,  
289 *Geophysical Research Letters*, p. e2022GL098856, 2022.
- 290 Kitoh, A., Endo, H., Krishna Kumar, K., Cavalcanti, I. F., Goswami, P., and Zhou, T.: Monsoons in a changing world: A regional perspective  
291 in a global context, *Journal of Geophysical Research: Atmospheres*, 118, 3053–3065, 2013.
- 292 Lee, D., Min, S.-K., Jin, J., Lee, J.-W., Cha, D.-H., Suh, M.-S., Ahn, J.-B., Hong, S.-Y., Kang, H.-S., and Joh, M.: Thermodynamic and  
293 dynamic contributions to future changes in summer precipitation over Northeast Asia and Korea: a multi-RCM study, *Climate dynamics*,  
294 49, 4121–4139, 2017.
- 295 Lee, J.-Y. and Wang, B.: Future change of global monsoon in the CMIP5, *Climate Dynamics*, 42, 101–119, [https://doi.org/10.1007/s00382-](https://doi.org/10.1007/s00382-012-1564-0)  
296 [012-1564-0](https://doi.org/10.1007/s00382-012-1564-0), 2014.
- 297 Lei, Y., Hoskins, B., and Slingo, J.: Exploring the interplay between natural decadal variability and anthropogenic climate change in summer  
298 rainfall over China. Part I: Observational evidence, *Journal of Climate*, 24, 4584–4599, 2011.

299 Li, J., Zhao, Y., Chen, D., Kang, Y., and Wang, H.: Future precipitation changes in three key sub-regions of East Asia: the roles of thermo-  
300 dynamics and dynamics, *Climate dynamics*, pp. 1–22, 2021.

301 Li, X., Ting, M., Li, C., and Henderson, N.: Mechanisms of Asian Summer Monsoon Changes in Response to Anthropogenic Forcing in  
302 CMIP5 Models\*, *Journal of Climate*, 28, 4107–4125, <https://doi.org/10.1175/jcli-d-14-00559.1>, 2015.

303 Lu, R. and Fu, Y.: Intensification of East Asian summer rainfall interannual variability in the twenty-first century simulated by 12 CMIP3  
304 coupled models, *Journal of Climate*, 23, 3316–3331, 2010.

305 Masson-Delmotte, V., P., Zhai, A., Pirani, S. L., Connors, C., Péan, S., Berger, N., Caud, Y., Chen, L., Goldfarb, M. I., Gomis, M., Huang,  
306 K., Leitzell, E., Lonnoy, J. B. R., Matthews, T. K., Maycock, T., Waterfield, O., Yelekçi, R. Y., and Zhou, B.: IPCC: Climate Change 2021:  
307 The Physical Science Basis. Contribution of Working Group I to the Sixth Assessment Report of the Intergovernmental Panel on Climate  
308 Change, Cambridge University Press, 2021.

309 Moon, S. and Ha, K.-J.: Future changes in monsoon duration and precipitation using CMIP6, *npj Climate and Atmospheric Science*, 3, 1–7,  
310 <https://doi.org/10.1038/s41612-020-00151-w>, 2020.

311 O’Neill, B. C., Tebaldi, C., Van Vuuren, D. P., Eyring, V., Friedlingstein, P., Hurtt, G., Knutti, R., Kriegler, E., Lamarque, J.-F., Lowe, J.,  
312 Meehl, J., Moss, R., Riahi, K., and Sanderson, B. M.: The scenario model intercomparison project (ScenarioMIP) for CMIP6, *Geoscientific*  
313 *Model Development*, 9, 3461–3482, <https://doi.org/10.5194/gmd-9-3461-2016>, 2016.

314 O’Neill, B. C., Kriegler, E., Ebi, K. L., Kemp-Benedict, E., Riahi, K., Rothman, D. S., van Ruijven, B. J., Van Vuuren, D. P., Birkmann, J.,  
315 Kok, K., Levy, M., and Solecki, W.: The roads ahead: Narratives for shared socioeconomic pathways describing world futures in the 21st  
316 century, *Global Environmental Change*, 42, 169–180, <https://doi.org/10.1016/j.gloenvcha.2015.01.004>, 2017.

317 Park, J., Kim, H., Wang, S.-Y. S., Jung, J.-H., Lim, K.-S., and Yoon, J.-H.: Long-term intensification of the East Asian Summer Monsoon  
318 (EASM) lifecycle based on observation and CMIP6, in: EGU General Assembly Conference Abstracts, p. 4359, 2020.

319 Qu, X., Huang, G., and Zhou, W.: Consistent responses of East Asian summer mean rainfall to global warming in CMIP5 simulations,  
320 *Theoretical and applied climatology*, 117, 123–131, 2014.

321 Seo, K.-H., Ok, J., Son, J.-H., and Cha, D.-H.: Assessing future changes in the East Asian summer monsoon using CMIP5 coupled models,  
322 *Journal of climate*, 26, 7662–7675, 2013.

323 Tebaldi, C., Debeire, K., Eyring, V., Fischer, E., Fyfe, J., Friedlingstein, P., Knutti, R., Lowe, J., O’Neill, B., Sanderson, B., Van Vuuren, D.,  
324 Riahi, K., Meinshausen, M., Nicholls, Z., Hurtt, G., Kriegler, E., Lamarque, J., Meehl, G., Moss, R., Bauer, S. E., Boucher, O., Brovkin,  
325 V., Golaz, J., Gualdi, S., Guo, H., John, J. G., Kharin, S., Koshiro, T., Ma, L., Olivie, D., Panickal, S., Qiao, F., Rosenbloom, N., Schupfner,  
326 M., Seferian, R., Song, Z., Steger, C., Sellar, A., Swart, N., Tachiiri, K., Tatebe, H., Voldoire, A., Volodin, E., Wyser, K., Xin, X., Xinyao,  
327 R., Yang, S., Yu, Y., and Ziehn, T.: Climate model projections from the Scenario Model Intercomparison Project (ScenarioMIP) of CMIP6,  
328 *Earth System Dynamics Discussions*, 2020, 1–50, <https://doi.org/10.5194/esd-2020-68>, 2020.

329 Van Vuuren, D. P., Kriegler, E., O’Neill, B. C., Ebi, K. L., Riahi, K., Carter, T. R., Edmonds, J., Hallegatte, S., Kram, T., Mathur, R., et al.:  
330 A new scenario framework for climate change research: scenario matrix architecture, *Climatic Change*, 122, 373–386, 2014.

331 Volonté, A., Muetzelfeldt, M., Schiemann, R., Turner, A. G., and Klingaman, N.: Magnitude, scale, and dynamics of the 2020 mei-yu rains  
332 and floods over China, *Advances in Atmospheric Sciences*, 38, 2082–2096, 2021.

333 Wang, B., Yim, S.-Y., Lee, J.-Y., Liu, J., and Ha, K.-J.: Future change of Asian-Australian monsoon under RCP 4.5 anthropogenic warming  
334 scenario, *Climate dynamics*, 42, 83–100, 2014.

335 Wang, B., Jin, C., and Liu, J.: Understanding future change of global monsoons projected by CMIP6 models, *Journal of Climate*, 33, 6471–  
336 6489, 2020.



337 Wang, B. et al.: Rainy season of the Asian–Pacific summer monsoon, *Journal of Climate*, 15, 386–398, 2002.

338 WCRP: CMIP6 data, <https://esgf-node.llnl.gov/search/cmip6/>.

339 Wilcox, L. J., Liu, Z., Samset, B. H., Hawkins, E., Lund, M. T., Nordling, K., Undorf, S., Bollasina, M., Ekman, A. M., Krishnan, S., et al.:  
340 Accelerated increases in global and Asian summer monsoon precipitation from future aerosol reductions, *Atmospheric Chemistry and*  
341 *Physics*, 20, 11 955–11 977, 2020.

342 Xin, X., Wu, T., Zhang, J., Yao, J., and Fang, Y.: Comparison of CMIP6 and CMIP5 simulations of precipitation in China and the East Asian  
343 summer monsoon, *International Journal of Climatology*, 40, 6423–6440, 2020.

344 Xue, D., Lu, J., Leung, L. R., Teng, H., Song, F., Zhou, T., and Zhang, Y.: Robust projection of East Asian summer monsoon rainfall based  
345 on dynamical modes of variability, *Nature Communications*, 14, 3856, 2023.

346 Yihui, D., Yanju, L., and Yafang, S.: East Asian summer monsoon moisture transport belt and its impact on heavy rainfalls and floods in  
347 China, , 31, 629–643, 2020.

348 Yu, T., Chen, W., Gong, H., Feng, J., and Chen, S.: Comparisons between CMIP5 and CMIP6 models in simulations of the climatology and  
349 interannual variability of the east asian summer Monsoon, *Climate Dynamics*, 60, 2183–2198, 2023.

350 Ziese, M. et al.: GPCP Full Data Daily Version 2020 at 1.0°: Daily Land-Surface Precipitation from Rain-Gauges built on GTS-based and  
351 Historic Data., 10.5676/DWD\_GPCC/FD\_D\_V2020\_100, 2020.